ADVANCED FUNCTIONAL MATERIALS
www.afm-journal.de

Ultrafast Transient Absorption Studies of the Dynamics of Free and Coulombically Trapped Polarons in Doped Conjugated Polymers

Eric C. Wu, Diego Garcia Vidales, Charlene Z. Salamat, Quynh M. Duong, Alex León Ruiz, Austin D. Ready, Zerina Mehmedović, Dane A. Stanfield, Alexander M. Spokoyny, Sarah H. Tolbert, and Benjamin J. Schwartz**

The relaxation of photoexcited polarons in doped conjugated polymers is studied with ultrafast transient absorption (TA) spectroscopy to examine the effect of polymer morphology and counterion size on polaron mobility. Processing conditions are first used to create F_4TCNQ-doped (2,3,5,6-tetrafluoro-tetracyanoquinodimethane) poly(3-hexylthiophene-2,5-diyl) (P3HT) films with different morphologies and thus free and trapped polarons in different ratios. We find that less crystalline films have a higher fraction of trapped polarons, but, remarkably, that free and trapped polarons have the same relaxation times in all films. Films doped with a large dodecaborane (DDB) cluster-based dopant are then used to show that trapping is based on Coulomb interactions between polarons and counterions; no trapped polarons are observed in TA due to the reduced Coulomb interaction between the polarons and the DDB counterion. Indeed, the relaxation of polarons in these films is an order of magnitude faster than that in F_4TCNQ-doped films, consistent with reduced trapping. Finally, the results are used to argue that counterion size has a greater effect on polaron mobility than polymer morphology and crystallinity. All of the experiments show that pump/probe spectroscopy provides a straightforward way to determine the local mobilities and degree of carrier trapping in doped conjugated polymer films.

1. Introduction

Organic semiconductors, such as conjugated polymers, have low intrinsic carrier densities. To improve their electrical conductivity, charge carriers, i.e., holes or electrons, can be added to their π-systems via doping. For chemical doping of poly(3-hexylthiophene-2,5-diyl) (P3HT; **Figure 1a**), a commonly studied *p*-type conjugated organic polymer, strong oxidants, such as 2,3,5,6-tetrafluoro-7,7,8,8-tetracyanoquinodimethane, F_4TCNQ (also shown in Figure 1a), are used to remove electrons from the π-conjugated backbone. When an electron is removed, the polymer backbone undergoes an aromatic-to-quinoidal structure change; the positive charge, the unpaired electron that remains, and the locally distorted quinoidal backbone structure are together referred to as a polaron. This paper focuses on using ultrafast transient absorption (TA) spectroscopy to uncover the microscopic details of how polarons in different environments have different local mobilities based on both the overall polymer morphology and the choice of dopant counterion.

The left panel of Figure 1c shows that the structural rearrangement associated with doping causes two states to move into the bandgap (BG), creating two new optical transitions.[1–9] The lower-energy P1 band results from a transition between the valence band and the lower charge-induced intragap state; this transition usually occurs near 0.5 eV for doped P3HT, although the precise energy of this band is related to the delocalization length of the polaron.[9–11] The higher-energy P2 band, typically observed near 1.5 eV for doped P3HT, results from a transition between the lower and upper intragap states. The energy diagram in Figure 1c also suggests the possible existence of two more absorption features, P3 and P3´, which are usually forbidden by symmetry.[12–14] However, if polarons delocalize across multiple chains, the P3 and P3´transitions can become partly allowed.[6,12,13] Although the electronic structure picture shown in Figure 1c has been challenged,[15,16] both ultrafast

E. C. Wu, D. G. Vidales, C. Z. Salamat, Q. M. Duong, A. León Ruiz, A. D. Ready, Z. Mehmedović, D. A. Stanfield, A. M. Spokoyny, S. H. Tolbert, B. J. Schwartz
Department of Chemistry and Biochemistry
University of California
Los Angeles, CA 90095–1569, USA
E-mail: tolbert@chem.ucla.edu; schwartz@chem.ucla.edu
S. H. Tolbert
Department of Materials Science and Engineering
University of California
Los Angeles, CA 90095–1569, USA
The ORCID identification number(s) for the author(s) of this article can be found under https://doi.org/10.1002/adfm.202507480

DOI: 10.1002/adfm.202507480

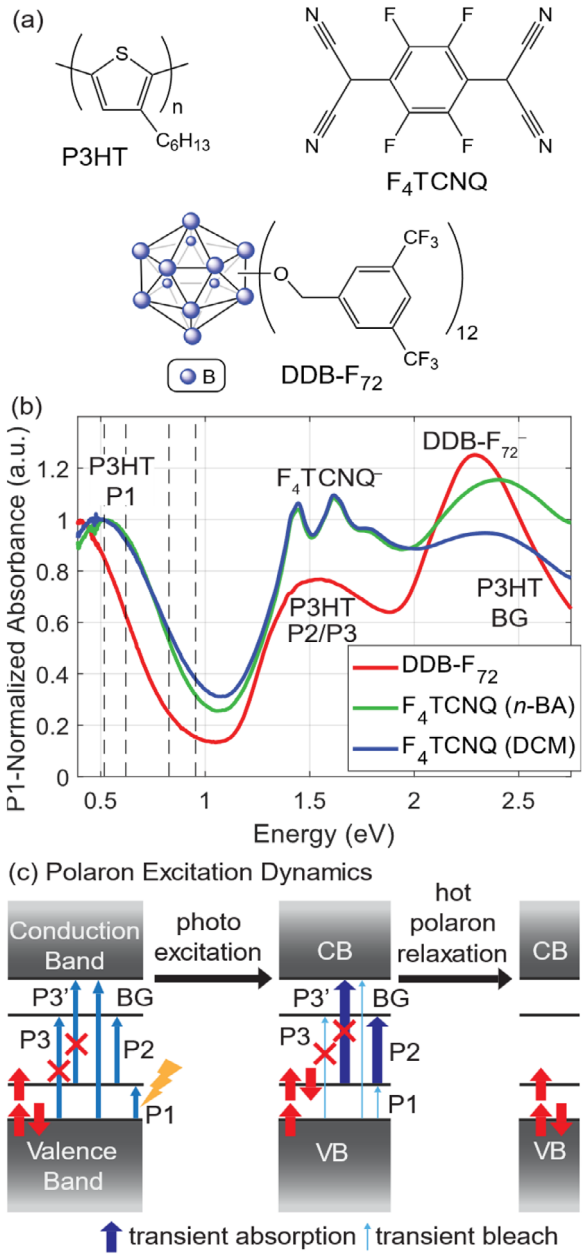

Figure 1. a) Chemical structures of P3HT, F_4TCNQ, and DDB-F_{72}. b) UV–vis–NIR absorption spectra of P3HT doped with: DDB-F_{72} (red), F_4TCNQ from *n*-butylacetate (*n*-BA, green), and F_4TCNQ from dichloromethane (DCM, blue). The spectra are normalized by the absorbance of the P1 peak near 0.5 eV. The vertical dashed lines indicate the pump wavelengths used in the transient absorption experiments, which are 1300, 1500, 2000, and 2400 nm. c) Energy diagrams showing the optical transitions (left panel) and polaron excitation dynamics of doped conjugated polymers. The P3 and P3´transitions in doped polymers are forbidden by symmetry, as indicated by red X's, but if the polaron delocalizes across multiple chains, these transitions can become partly allowed. Photoexcitation of the P1 transition promotes an electron from the valence band to the lower intra-gap state, which creates a transient absorption feature at the position of the P2 band and a transient bleach feature at the BG and P1 band (center panel). For a polaron that delocalizes across multiple chains, a transient absorption of the P3´band and a transient bleach of the P3 band can also be created. The transient absorption dynamics decay to zero when the polaron returns to its original state (right panel).

transient absorption (TA) spectroscopy experiments[17–21] and time-dependent density functional theory calculations with natural transition orbitals[9,22] have confirmed that this picture works well for describing the basic spectroscopic features of doped conjugated polymers.

When a conjugated polymer is doped, a counterion is introduced into the doped polymer to maintain electrical neutrality. The location and size of the counterion play an important role in determining both the mobility and the identity of the charge carriers.[10,23–26] We and others have argued that the distance between the polaron and counterion affects the degree of polaron delocalization and thus the energetic location of the P1 peak.[10,23,26,27] If the counterion size or local crystal structure brings the counterion closer to the polymer backbone and thus to the polaron, the Coulomb interaction between the two causes the polaron to be less delocalized, leading to a blueshifted P1 absorption and lower carrier mobility.[10] In contrast, if the anion is farther from the polaron, the Coulomb interaction is reduced and the polaron will be more delocalized, leading to a redshifted P1 absorption and a higher carrier mobility. We verified these ideas using a redox-active weakly-coordinating dodecaborane cluster-based dopant[28,29] (DDB-F_{72}, Figure 1a) that has a large enough physical size to minimize the Coulomb attraction between the anion and the polaron, producing a very redshifted P1 peak position (cf. red curve in Figure 1b) and a greatly increased carrier mobility in both doped conjugated polymers[23,30] and doped single-walled carbon nanotubes.[31] We note, however, that others have argued that polymer morphology, including structural disorder or the connectivity between domains, plays a more important role in determining carrier mobility than counterion size.[32–34]

One of the potential issues with correlating the P1 peak position and carrier mobility is that the P1 peak position is a measure of the local molecular environment of the polaron and its degree of delocalization, whereas common methods to determine carrier mobility, such as the Hall effect measurements, are performed on macroscopic length scales. We and others have argued that one can use ultrafast transient absorption (TA) spectroscopy to study the local mobility of carriers in doped P3HT films.[17–21] Photoexciting the P1 transition promotes a valence-band electron (i.e., an electron in the HOMO of an undoped polymer segment where the polaron is not located) into the hole: in other words, the P1 band is effectively a photoinduced charge transfer transition (see the upper diagrams in **Figure 2**). This creates both a positively-charged aromatic polymer segment and a neutral quinoidal segment (second row of diagrams in Figure 2). The positively-charged aromatic segment will undergo the aromatic-to-quinoidal transformation to stabilize the positive charge, which will migrate to a nearby stable location ("cooling" of the newly-created "hot" polaron), while the now-neutral quinoidal segment will undergo a quinoidal-to-aromatic transformation (third row of diagrams in Figure 2). This backbone rearrangement process takes place in less than 1 ps. We note that photoexcitation of the P1 transition leads to TA signatures that are easier to interpret than photoexcitation of other transitions because one can cleanly excite polarons without interference from other processes, such as photoinduced charge transfer from the anion to the polymer backbone, or from other species, such as excitons or triplet excited states.[35]

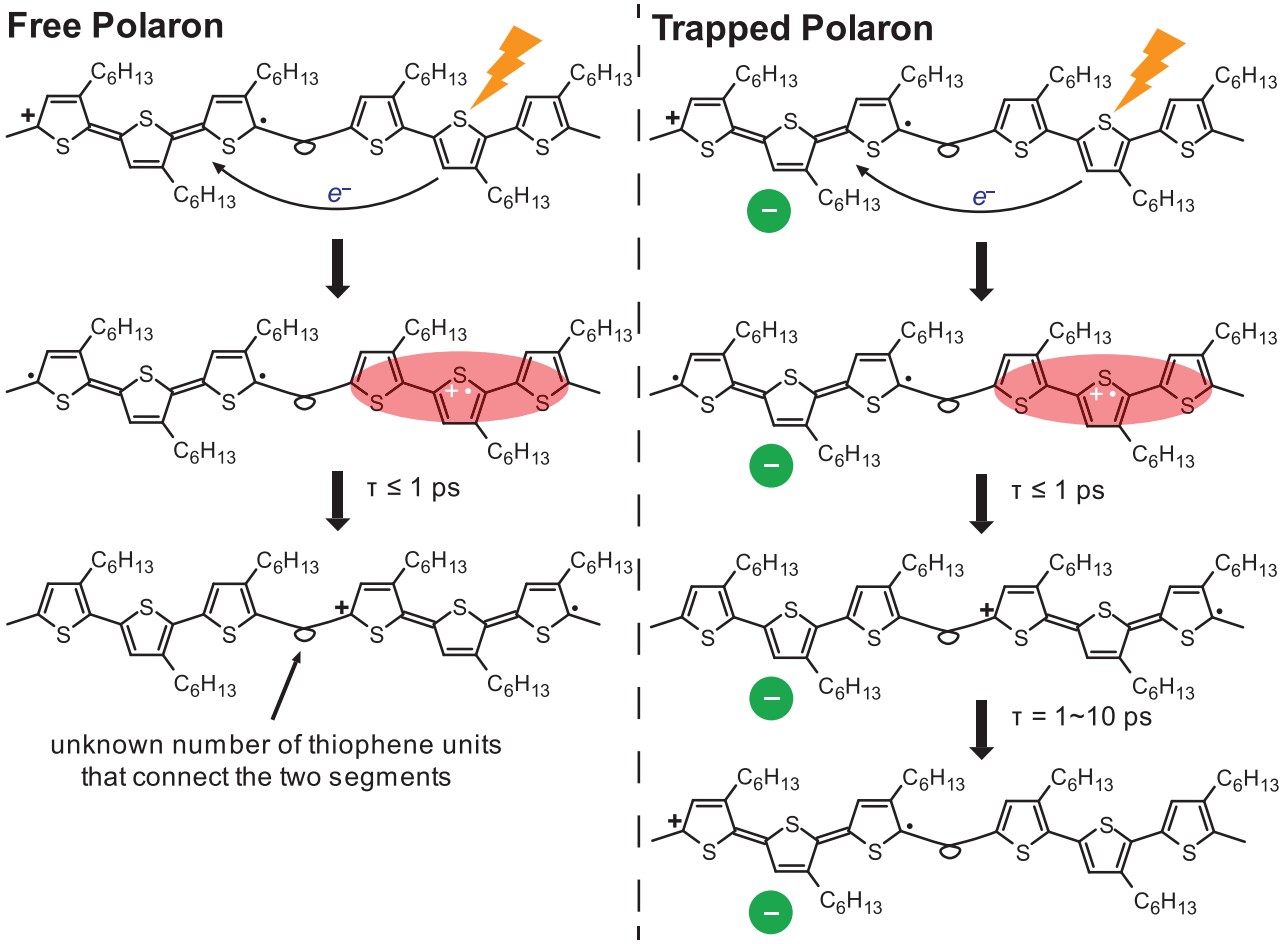

Figure 2. Schematic representation of our TA measurements that capture the difference between free polarons and Coulomb-trapped polarons. The loop represents an unknown number of P3HT monomers that connect the two segments. When the P1 peak is excited, an electron is transferred from the valence band (a neutral aromatic segment of the polymer) to the half-filled intragap state (a positively charged quinoidal segment of the polymer with a radical), as depicted in the upper panels. This electron transfer creates a positively charged radical aromatic segment (a "hot" delocalized polaron) and a neutral quinoidal segment, as shown in the second row of panels. The relaxation of the newly created hot polaron, including the aromatic-to-quinoid transformation, takes place in under a ps, as depicted in the third row of panels. For excitation of a free polaron (left panels), once the polaron has relaxed in its new location, the system is back at equilibrium and the TA signal disappears. However, for excitation of a Coulomb-trapped polaron (right panels), the polymer is not back at equilibrium following the initial polaron relaxation because the charge is now far from its initial counterion. This means that the absorption of the newly relaxed polaron is different from its initial absorption, so the TA signal persists until the polaron either migrates back to its initial location or finds an equivalent coulomb trap with another anion, a process that can take several ps.

If the initially excited polaron is highly delocalized or "free," the doped polymer at this point would be back at equilibrium. This means that the TA signal should decay to zero once this step is complete because the absorption spectrum of a free polaron, which means a polarized charge that is not Coulombically bound to its counterion, is the same regardless of its location (left diagrams in Figure 2). On the other hand, if the photoexcited polaron is initially Coulomb-trapped by a counterion, after photoinduced charge transfer and cooling, the polaron will now be located away from its initial counterion, which means that it will have a different degree of delocalization and thus a different absorption spectrum. This means that the TA signal will persist until the polaron migrates back to its initial location or to an equivalent counterion (right diagrams in Figure 2). The rate at which the newly cooled hole migrates depends on both the distance of the initial charge transfer and the local carrier mobility.

Figure 1c shows that photoexcitation of the P1 transition of a doped conjugated polymer creates a transient absorption feature at the position of the P2 band so that the dynamics of the induced P2 band serve as a measure of the local carrier mobility.[17,21] Indeed, we found previously that when we photoexcite the P1 band on its blue side, where more localized/deeply trapped polarons absorb, the decay of the induced P2 TA signal slows.[17] Conversely, when the P1 peak is excited on its red side, accessing less Coulomb-trapped and more free polarons, the decay of the TA signal is more rapid.[17] A careful analysis using singular value decomposition (SVD) allowed us to separate the TA spectra and the dynamics of both free and Coulomb-trapped polarons, and the pump-wavelength dependence of the TA signal allowed us to construct action spectra for how each of these species contributes to the overall P1 absorption band.[17]

Previously, Grieco and coworkers separately examined the effects of polymer morphology[20] and counterion size[21] using TA spectroscopy. These researchers also observed that the induced P2 peak area kinetics exhibit a biphasic decay following the excitation of P1, indicating the presence of free and trapped polarons in doped P3HT films with different morphologies[20] and different counterions.[21] Greico and co-workers altered the polymer film morphology by blending P3HT with another polymer that is electronically inert and disrupts P3HT crystallization. They showed that this disruption of crystallinity creates more trapped polarons, slowing the relaxation of the TA signal.[20] In a separate paper,[21] however, they also reported a lack of a clear correlation between the P1 peak position and TA relaxation time when they doped P3HT films with different counterions.

In this paper, we use ultrafast TA spectroscopy to learn more about the nature of the charge carriers in doped P3HT films, correlating the TA results with macroscopic measures of carrier mobility. Our work extends previous studies[17–21] in two new directions. First, we examine how the morphology/degree of crystallinity of the doped polymer affects the dynamics of the free and Coulomb-trapped polarons, which we accomplish not by the addition of another polymer, but by using different processing methods to infiltrate traditional F_4TCNQ dopants into P3HT films. Second, we perform ultrafast TA experiments on DDB-F_{72}-doped P3HT films to determine how the interplay of counterion size and polymer morphology affects the nature of the charge carriers. This allows us to directly address the question as to whether or not the polarons in DDB-F_{72}-doped films are indeed locally free, as we have argued previously,[23] or if there are TA signatures showing that some polarons are still coulombically trapped. Moreover, by comparing the relaxation time scales of photoexcited polarons in F_4TCNQ-doped and DDB-F_{72}-doped P3HT films, we can directly compare how Coulomb trapping by the counterion and local disorder each influence charge transport.

We find that although the morphology of the film does affect the ratio of free and Coulomb-trapped polarons, there is no easy route to eliminate the presence of Coulomb-trapped polarons solely by controlling film morphology. The free and Coulomb-trapped polarons in F_4TCNQ-doped films have similar TA dynamics regardless of infiltration method, but the ratio of free to Coulomb-trapped polarons does depends on the processing method, which controls the film morphology. On the other hand, we find that there are no signatures of Coulomb-trapped polarons in P3HT films doped with DDB-F_{72}. The time constant for the decay of the TA signal for DDB-F_{72}-doped films is an order of magnitude faster than that of the Coulomb-trapped polarons in F_4TCNQ-doped films. This shows that counterion size provides a more straightforward way than morphology to eliminate counterion-based Coulomb trapping of polarons in doped conjugated polymer films.

2. Results and Discussion

For all of the work described below, we prepared doped P3HT films by sequential processing (SqP),[10,36–39] where undoped P3HT films were first made by spin coating, and then the dopant (either F_4TCNQ or DDB-F_{72}) was introduced in a second spin coating step from a semi-orthogonal solvent (*n*-butylacetate, *n*-BA, or dichloromethane, DCM) that swells but does not dissolve the underlying polymer film. We chose *n*-BA and DCM based on a trade-off between their ability to swell the polymer and their vapor pressures. DCM swells the polymer better but has a much higher vapor pressure; this causes it to create a more disordered doped film than *n*-BA, which does not swell the polymer as well but has a lower vapor pressure. Because *n*-BA and DCM have very different vapor pressures and swelling abilities for P3HT, they create doped films with different morphologies,[25,40,41] as discussed further below. We used only DCM for doping P3HT films with DDB-F_{72} because of the limited solubility of DDB-F_{72} in *n*-BA. Details of film fabrication and other experimental details are given in the Supporting Information (SI).

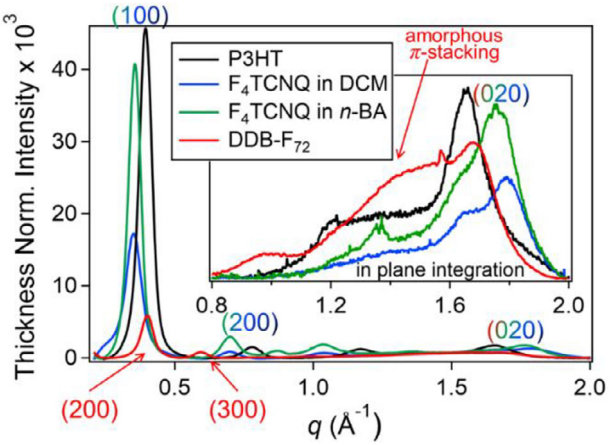

Figure 3. Radially integrated, thickness-normalized 2-D GIWAXS diffractograms for undoped P3HT (black curve) and P3HT doped with DDB-F_{72} (red curve) and F_4TCNQ from either *n*-BA (green curve) or DCM (blue curve). The inset shows the in-plane integration, highlighting the (020) and amorphous π-stacking peaks. The relative intensities of the (100) peaks show that P3HT doped with F_4TCNQ from *n*-BA creates a more crystalline film than that doped with F_4TCNQ from DCM. The relative crystallinity of the DDB-F_{72}-doped films cannot be determined from the lamellar peak intensity, as the (100) peak is blocked by the beamstop, but the presence of a broad amorphous peak n1.4 $Å^{-1}$ suggests a significant disordered component in this sample.

2.1. Macroscopic Structure of Doped P3HT Films

Figure 3 shows radially-integrated GIWAXS diffractograms for the P3HT samples studied in this work. The 2D diffractograms from which these radial integrations were obtained are shown in Figure S1 (Supporting Information). For undoped P3HT (black curve) and the F_4TCNQ-doped P3HT samples created using different solvents (blue curve for DCM and green curve for *n*-BA), the (100) fundamental lamellar peak is located near 0.35 $Å^{-1}$, and the samples are ordered enough that two overtones are also visible. The diffractogram also shows an (020) π-stacking peak near 1.7 $Å^{-1}$ (Figure 3 inset). The F_4TCNQ-doped films show their (100) peak at a smaller *q* position and their (020) peak at a higher *q* position compared to the undoped films, reflecting the fact that the P3HT crystal structure changes in order to incorporate the F_4TCNQ^- anion into the lamellar region among the side chains.[10,36,42]

Table 1. Conductivity, Hall mobility, free carrier density, paracrystallinity ($g_{(hkl)}$)*, the time constants for fast and slow components, and percents of fast components for DDB-F_{72}-doped and two different F_4TCNQ-doped P3HT films.

	DDB-F_{72}	F_4TCNQ [*n*-BA]	F_4TCNQ [DCM]
Conductivity [S cm^{-1}]	7.33	2.47	2.55
Hall Mobility [cm^2 V^{-1} s^{-1}]	0.082	0.046	0.045
Carrier Density [cm^{-3}]***	5.6×10^{20}	3.3×10^{20}	3.6×10^{20}
$g_{(100)}$	0.16	0.15	0.17
τ [ps]	1.3	0.29/15.2	0.29/15.1
Percent of fast components for different pump wavelengths**	100%	70% (1300 nm) 75% (1500 nm) 79% (2000 nm) 82% (2400 nm)	40% (1300 nm) 44% (1500 nm) 52% (2000 nm) 62% (2400 nm)

*Paracrystallinity based on the relative widths of the (100) peak and its overtones. Paracrystallinity quantifies disorder within the P3HT crystallites.[43,44] **The numbers in the parenthesis are the pump wavelengths. ***Because of the large size of the DDB-F_{72} dopant, the DDB-F_{72}-doped films are roughly twice as thick as F_4TCNQ-doped films, so the density of thiophene monomers in the DDB-F_{72}-doped P3HT films is about half. Therefore, the number of charges/thiophene ring is 0.084 and 0.072 for the films doped with F_4TCNQ in *n*-BA and DCM, respectively, and 0.069 for the DDB-F_{72}-doped films.

For DDB-F_{72}-doped P3HT (red curve), instead of small shifts associated with doping, we see a different pattern of lamellar peaks appearing near 0.4 and 0.6 $Å^{-1}$. Based on the peaks' positions, we have concluded previously that these are the (200) and (300) peaks of a lamellar progression with a much larger spacing; the (100) fundamental peak should appear near 0.2 $Å^{-1}$, but that peak is not visible because it is blocked by the beamstop at low *q*.[23,24,30] In addition to new lamellar peaks, doping with DDB-F_{72} also creates a broad peak near 1.4 $Å^{-1}$, which we have previously assigned to amorphous scattering from disordered π-stacks.[23,24,30] The appearance of new lamellar and π-stacking peaks reflects a significant change in the doped polymer crystal structure due to the large size of DDB-F_{72} (≈2 nm diameter), which occupies such a significant amount of space that it nearly doubles the distance between the P3HT chains in the lamellar direction.[23,24,30]

In addition to the new peak positions that reflect changes in crystal structure induced by doping, the intensities (which are normalized by the film thickness) of the scattering peaks in Figure 3 show that doping also changes the degree of crystallinity of the P3HT films. For the F_4TCNQ-doped films, DCM, which has a higher vapor pressure and is a better swelling solvent for P3HT,[40] creates more disordered doped films than *n*-BA; this is seen directly by the much higher (100) peak for the doped film made using *n*-BA. Another measure of the amount of disorder in the P3HT crystallites is paracrystallinity, *g*, which is based on the relative widths of the lamellar scattering peaks.[43,44] **Table 1** shows a higher paracrystallinity for films doped with F_4TCNQ from DCM, again indicating that these films are more disordered than those doped using *n*-BA.

For DDB-F_{72}-doped films, the (100) peak is not visible due to beam scattering at low *q*, therefore, one cannot use the (100) peak intensity to compare the degree of crystallinity of F_4TCNQ-doped and DDB-F_{72}-doped films. However, the presence of a prominent disordered π-stacking peak, which is absent in F_4TCNQ-doped films, and the weak intensity of the crystalline (020) peak compared to the F_4TCNQ-doped films, indicate that doping with DDB-F_{72} creates a more disordered film than doping with F_4TCNQ. This makes sense in light of previous work that showed that the strain of intercalating the large DDB-F_{72} dopant can break up existing crystallites into smaller regions of varying sizes.[30]

2.2. Transient Absorption Spectra of Doped P3HT Films

Figure 4a shows the 2000 nm (0.62 eV)-pumped TA spectra of the DDB-F_{72}-doped and F_4TCNQ-doped P3HT films with two different morphologies at a delay time of 1 ps. The setup of the TA experiments is the same as in our previous work[17,18] and is described in detail in the Supporting Information. The TA spectra of all three doped samples show a positive peak (induced absorption) near 1.2 eV and negative peaks (transient bleaches) near 1.75 and 2.4 eV. Based on the peak assignments in the steady-state UV–vis–NIR spectra in Figure 1b, the positive peak around 1.2 eV is the induced P2 transition, and the negative peaks at 1.75 and 2.4 eV are bleaches of the P3 and BG transitions, respectively. These transient bleach and absorption patterns fit perfectly with the traditional electronic structure picture shown in Figure 1c: when one pumps the P1 transition, an electron is excited from the valence band to the lower intragap state, leading to a bleach of the P3 and BG transitions and an induced absorption of the P2 transition (see Figure S2, Supporting Information). We note that alternate pictures of the band structure of doped conjugated polymers[15,16] predict a bleach of the P2 transition and no P3 transition, contrary to what is observed here and in other work.[17,20,21]

The data in Figure 4a also show that P3HT films doped with DDB-F_{72} (red curve) and with F_4TCNQ from *n*-BA (green curve) have a positive TA peak around 1.9 eV; the film doped with F_4TCNQ from DCM (blue curve) also appears to show a similar feature, although it is much smaller and largely swamped out the bleach signal near 2.4 eV. This type of positive-going TA feature has been previously observed by Grieco and co-workers, who assigned it as an electroabsorption (EA) signal caused by the electric field created when the photoexcitation of the P1 transition separates the hole from its counterion (cf. right-hand diagrams, Figure 2).[19–21] This photoinduced electric field shifts the bandgap absorption of nearby undoped polymers, creating a derivative-like feature near the bandgap in the TA difference spectrum (see Figure S3, Supporting Information). Indeed, we see a striking similarity between the positive TA feature near 2 eV and

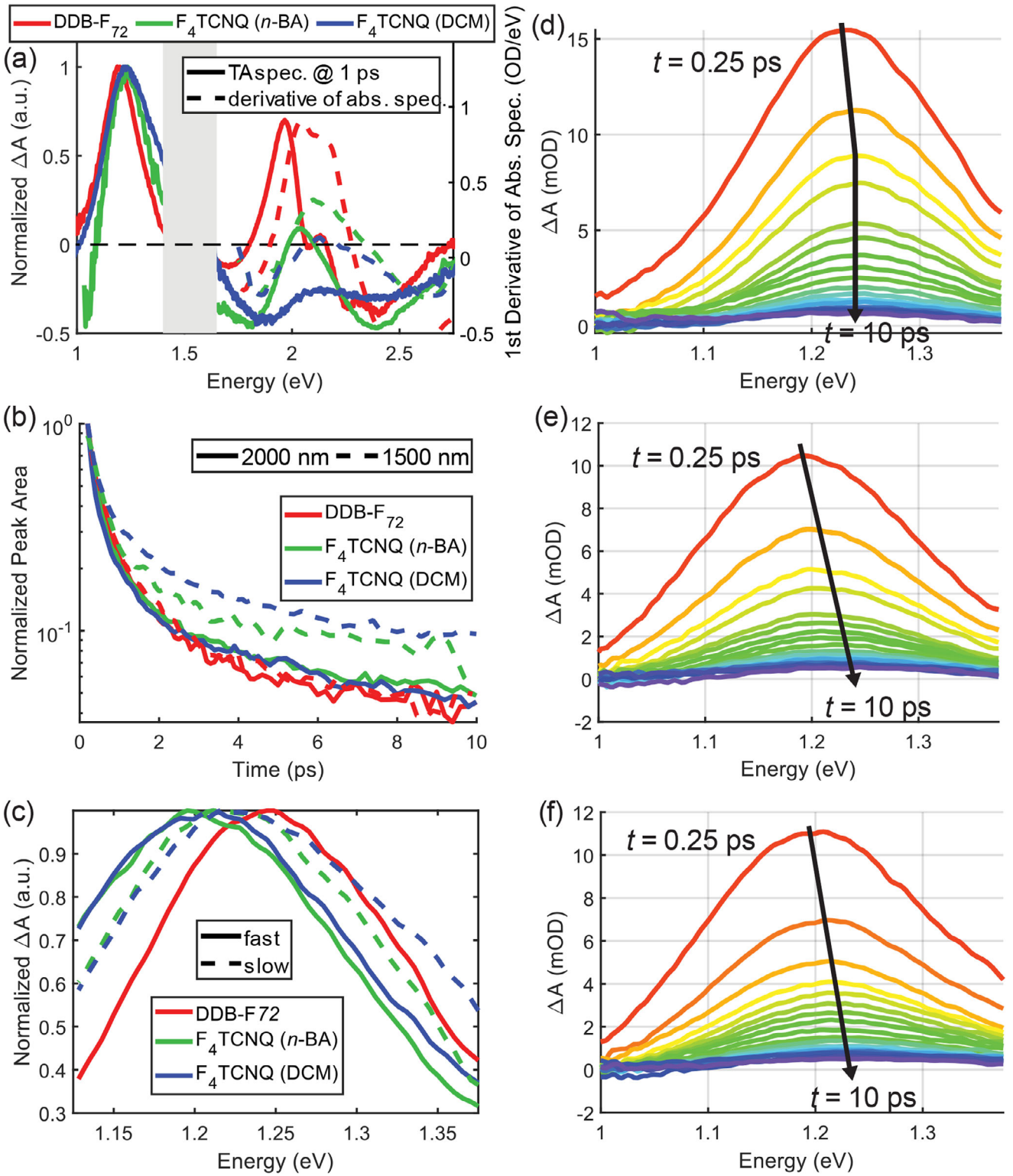

Figure 4. a) TA spectrum of doped P3HT films at 1 ps following excitation at 2000 nm. The dashed curves are the derivative of the steady-state absorption spectra shown in Figure 1b; the strong resemblance to the TA signal in the 2 eV region indicates that the 2 eV feature results from electroabsorption.[19,20] The TA spectrum is not shown in the region near 1.5 eV due to scatter from the beam fundamental. b) The normalized P2 peak (≈1.2 eV TA feature) integrated area as a function of time for DDB-F_{72}-doped (red curves) and F_4TCNQ-doped (blue and green curves) P3HT films following excitation at 1500 nm (dashed curves) and 2000 nm (solid curves). c) Spectral components of DDB-F_{72}-doped and F_4TCNQ-doped P3HT films extracted from SVD fitting using all 4 excitation wavelengths. Time evolution of the TA spectrum in the P2 region of P3HT films doped with DDB-F_{72} d) and F_4TCNQ in *n*-BA e) and DCM f) following excitation at 2000 nm; the different time traces are spaced logarithmically from 0.25 ps (red) to 10 ps (purple).

the derivative of the steady-state absorption spectrum, shown as the dashed curves in Figure 4a, in agreement with the assignment of this feature as arising from an EA signal.[19–21]

We note that in previous work,[17] we did not observe transient EA features when exciting P3HT films doped with F_4TCNQ from DCM. However, the films we studied in Ref. [17] were heavily doped and had steady-state absorption spectra that were essentially flat in this region. This means that any EA signals, which would have looked like the derivative of a relatively flat curve, would have been much smaller than those seen here.

One of the difficulties in untangling the carrier dynamics associated with the excitation of the polaron P1 transition is that the bleach of the P3 transition, the electroabsorption signal, and the bleach of the BG transition all strongly overlap. Thus, for the remainder of this work, we will focus primarily on the dynamics of the induced P2 transition near 1.2 eV to study the nature of the photoexcited polarons in our different doped P3HT films. Figure 4 shows the evolution of the TA spectra from 0.25 to 10 ps in the induced P2 region for DDB-F_{72}-doped (panel d), F_4TCNQ in *n*-BA doped (panel e), and F_4TCNQ in DCM doped (panel f) P3HT films following P1 excitation at 2000 nm. Figure 4b shows the integrated peak area of this feature for both 2000 nm (0.62 eV, solid curves) and 1500 nm (0.83 eV, dashed curves) excitation as a function of time for all three films. Since the widths of the induced P2 peaks are different, the peak areas were integrated over the full width at half maximum (FWHM).

Figure 4d–f shows that as the photoinduced P2 TA peak decays, it also blueshifts for both of the F_4TCNQ-doped P3HT films. For the DDB-F_{72}-doped sample, the magnitude of the blueshift is much smaller and is completed by a delay time of 0.50 ps (Figure 4d; Figure S4a, Supporting Information, yellow curve). In addition, Figure 4b shows that the decay rate is pump-wavelength dependent for both F_4TCNQ-doped films, but not pump-wavelength dependent for P3HT doped with DDB-F_{72}. For both F_4TCNQ-doped films, the induced P2 TA signal decays more slowly as the pump wavelength is tuned to the blue from 2000 to 1500 nm. The more disordered P3HT film doped with F_4TCNQ from DCM shows the slowest P2 decay of all the samples when excited at 1500 nm.

To extract the dynamics of the free and Coulomb-trapped polarons in these doped P3HT films, we used singular value decomposition (SVD) to examine the number of underlying spectral components in the TA signals of each sample from all 4 excitation wavelengths. SVD analysis separates the induced P2 TA spectra into underlying spectral and kinetic components; when applied to our TA data, SVD showed that there were two well-defined components for the F_4TCNQ-doped samples, but only one component (excluding a faster-than-instrument-limited feature; see the Supporting Information for details) for DDB-F_{72}-doped P3HT. We used a least-squares fitting procedure (also described in the Supporting Information) to fit single-exponentially decaying kinetics to each component, which turned out to have different time constants: one fast and one slow. Based on the discussion above, we assign the fast and slow components to the cooling of the initially created hot polarons and the migration of Coulomb-trapped polarons back to their original sites, respectively.[17] Figure 4c shows the SVD-extracted absorption spectra of the spectral components for each sample. Table 1 lists the decay time constants of the different components for each sample and excitation wavelength, in addition to macroscopic charge transport characteristics that we measured for these same doped P3HT samples.

2.3. Discussion

Table 1 shows that the two F_4TCNQ-doped films show similar behavior for a series of macroscopic measurements, including electrical conductivity, Hall carrier mobility, and carrier density (Table 1), but the TA measurements show that the two films have somewhat different microscopic behavior. We note that both the Semi-Localized Transport (SLoT) model[45] and the Kang–Snyder (K–S) model[46] predict that carrier mobility should increase as the carrier density increases. This means that when working to understand the effects of polymer morphology and counterion size on carrier mobility, one must ensure that the samples have a similar carrier density, as we have done here. We find that the decay time constants of the fast and slow spectral components are similar for both films, but the amplitude ratios of the fast and slow spectral components are different for the F_4TCNQ-doped P3HT films made using the two different solvents. This suggests that the different solvents, which change the polymer morphology, are not significantly changing the cooling dynamics of hot polarons (fast component) or the mobility of Coulomb-trapped polarons that need additional relaxation (slow component), but instead are changing the relative populations of free polarons, which only show the fast component, and Coulomb-trapped polarons, which show both.

The amplitude ratio of the fast and slow spectral components for the two F_4TCNQ-doped P3HT films show that films doped from DCM, which are more disordered, have more Coulomb-trapped polarons (slow component) than films doped from *n*-BA. This observation is consistent with the fact that the P1 absorption band of the P3HT film doped with F_4TCNQ from DCM is broader on the blue side, where more trapped polarons absorb, than the film doped with F_4TCNQ from *n*-BA (cf. Figure 1b). This also confirms our previous observation[10] that in less crystalline films, more F_4TCNQ anions sit closer to the polarons when the structural constraints of a highly crystalline lattice are relaxed, so that less crystalline films have more Coulomb-trapped polarons.

We also performed electrical measurements, including electrical conductivity and Hall effect measurements, on the same films used for the ultrafast TA experiments, with the results summarized in Table 1. We find that not only do the two F_4TCNQ-doped films have similar time constants for the slow components, but they also have similar Hall carrier mobilities. This makes sense because the macroscopic mobilities measured by the Hall effect should be correlated with the slow spectral component, as it is this time constant that measures polaron diffusion, rather than polaron cooling.

One of the key findings of this work is that for DDB-F_{72}-doped P3HT films, there is no slow spectral component in the TA, indicating that there are essentially no Coulomb-trapped polarons in these films. In other words, effectively all of the polarons in DDB-F_{72}-doped P3HT films are free polarons. We note that Greico and co-workers recently performed TA experiments on P3HT films doped with different counterions, and found that for all the counterions they investigated the TA has both fast and slow relaxation

components.[21] Thus, our DDB-F_{72}-doped P3HT films are the only ones reported to date that do not show signatures of trapped polarons. The TA of our DDB-F_{72}-doped films has a decay time constant of 1.3 ps, which is an order of magnitude faster than the slow spectral component seen in the F_4TCNQ-doped films. This decay time constant agrees well with the polaron cooling time reported by Roy et al., who studied the aromatic-to-quinoid relaxation of polarons created in undoped P3HT films via ultrafast stimulated Raman spectroscopy.[47] Thus, in our DDB-F_{72}-doped films, we see only cooling of the newly created hot polarons (left side of Figure 2) and not relocalization of polarons back to their trap sites (lower right of Figure 2) because the size of the DDB dopant is large enough to prevent significant coulomb interaction with the polarons, meaning that the polarons are essentially all free.[23,24,30]

The absence of significant amounts of Coulomb-trapped polarons also explains why the TA decay rate of DDB-F_{72}-doped P3HT films is not pump wavelength dependent (Figure 4b). Because Coulomb-trapped polarons are more localized and thus have a bluer P1 absorption, tuning the excitation wavelength to the blue usually excites a higher fraction of trapped polarons and a lower fraction of the more delocalized free polarons, as seen with the F_4TCNQ-doped films as summarized in Table 1. Since there are effectively no Coulomb-trapped polarons in DDB-F_{72}-doped P3HT films, changing the pump wavelength cannot change the ratio of photoexcited free and trapped polarons, leading to a quickly-decaying TA signal that is pump wavelength independent. The absence of Coulomb-trapped polarons also explains the higher Hall carrier mobility of the DDB-F_{72}-doped P3HT films (Table 1) and is consistent with the very redshifted P1 absorption peak.

We note that in their recent work, Greico and co-workers did not see a clear correlation between the P1 peak position and TA relaxation time when they doped P3HT films with different counterions.[21] We believe this is because they used only a single excitation wavelength for all of their measurements, and did not spectrally separate the fast and slow relaxation components. The single excitation wavelength means that with counterions that produce highly redshifted P1 bands, they were selectively exciting the most trapped polarons in the sample, while with ions that yield blueshifted P1 bands, they were selectively exciting freer polarons. This change in relative excitation energy, along with the fact that the two spectral components were integrated together, likely obscured the strong correlation between the P1 position and TA relaxation time that we observe here.

As mentioned above, macroscopic measurements, such as electrical conductivity and Hall carrier mobility, are effectively rate-limited by the slower Coulomb-trapped polarons. Since the single decay time constant measure for the DDB-F_{72}-doped films is significantly faster than the slow component of the F_4TCNQ-doped films, this helps explain why both the Hall mobility and the conductivities of the DDB-F_{72}-doped films are higher than those of the F_4TCNQ-doped films. However, even though the decay time constant of the DDB-F_{72}-doped films is an order of magnitude faster than the slow component of F_4TCNQ-doped films, the Hall mobility of the DDB-F_{72}-doped films is only twice as high as the Hall mobility of the F_4TCNQ-doped films. This is likely because TA spectroscopy primarily measures local, microscopic mobility, while the Hall effect and electrical conductivity report on longer-ranged macroscopic mobility. Grain boundaries and the relative sizes of the crystalline and amorphous domains will also strongly affect macroscopic mobility, reducing the direct correlation.

We note that Table 1 shows that the single decay time constant of the P2 TA feature in the DDB-F_{72}-doped P3HT films is slower than the fast component measured for F_4TCNQ-doped films. This may be in part because the free carriers in the films doped by DDB-F_{72} are slightly less free than those in films doped by F_4TCNQ because the DDB-F_{72}-doped films are more disordered by the process of incorporating the very large dopant counterions into the P3HT crystallites.[23,24] In other words, the fast "cooling" relaxation component may involve some small component of migratory behavior that is slower in the more disordered DDB-F_{72}-doped samples.

Alternatively, the difference in time constants may arise from the nature of the fitting. For free polarons (left side of Figure 2), relaxation after photoexcitation involves mainly the aromatic-to-quinoidal transformation to stabilize the positive charge. On the other hand, for Coulomb-trapped polarons (right side of Figure 2), relaxation after photoexcitation involves both the aromatic-to-quinoidal transition and migration of the polarons to a new, stable location. In F_4TCNQ-doped films, the timescales for these two processes, aromatic-to-quinoid transition versus polaron migration, are distinct and show up as two different well-defined components in our SVD analysis. Thus, it makes sense that the fast component in the F_4TCNQ-doped films can be assigned to the cooling of the "hot" polaron through the aromatic-to-quinoid transformation and the slow component can be assigned to the migration of the polarons to the most stable location. In contrast, the timescales for these two processes may not be as distinct in DDB-F_{72}-doped films due to the lack of Coulomb-trapped polarons, so the single component seen in the SVD analysis comprises a mixture of both the aromatic-to-quinoid "cooling" and some small amount of polaron migration. Since the aromatic-to-quinoid "cooling" time should not be strongly affected by the disorder, this latter interpretation seems more plausible to explain the factor of 5 difference between the time constants associated with the fast component of the F_4TCNQ-doped films and that of the DDB-F_{72}-doped films. More importantly, the factor of ≈11 difference between the time constants associated with the slow component of the highly-crystalline F_4TCNQ-doped films and that of the DDB-F_{72}-doped films that contain a large disorder component indicates that Coulomb trapping plays a more significant role on local charge transport than does local disorder, even though both are clearly important.[23,24]

3. Conclusion

In summary, we performed ultrafast TA measurements on P3HT films doped with two different dopants, F_4TCNQ and DDB-F_{72}, to study how polymer morphology and counterion size affect the nature of polarons. The TA spectra were collected by exciting the polaron P1 transition, which moves an electron from the valence band, i.e., a neutral aromatic segment of the polymer, to the lower intragap state, i.e., a positively charged quinoidal segment of the polymer where the polaron is located. This creates a positively-charged aromatic segment, i.e., a "hot" polaron, that cools as the polymer backbone undergoes the aromatic-to-quinoidal

transformation. For free polarons, the cooling process returns the polymer back to equilibrium. For Coulombically-trapped polarons, those that reside near enough to a counterion to be somewhat localized, the initial cooling process does not return the polymer back to equilibrium because the polaron now resides at a different distance from the counterion. This leads to a second, slower induced P2 TA decay, reflecting the time needed for the polaron to either migrate back to its original counterion or find another counterion to return to equilibrium.

SVD analysis of the TA spectra showed that DDB-F_{72}-doped films display only a single polaron relaxation time, a time that is more than an order of magnitude faster than the slow TA component of F_4TCNQ-doped films; this suggests that the polarons in the DDB-F_{72}-doped films are much freer. This is also consistent with our observation that the polaron lifetime in DDB-F_{72}-doped films, unlike F_4TCNQ-doped films, is not pump wavelength dependent, suggesting a general lack of Coulomb-trapped polarons in DDB-F_{72}-doped films. If the fast relaxation time in the F_4TCNQ-doped films is assumed to be the "hot" polaron cooling through the aromatic-to-quinoid transition, the single TA relaxation rate of the DDB-F_{72}-doped films are only ≈4–5 times slower than that fast rate observed in F_4TCNQ-doped films, indicating that minimal polaron migration is needed to reach equilibrium in the DDB-F_{72}-doped films. This very fast relaxation occurs despite the fact that the DDB-F_{72}-doped films are more locally disordered than the F_4TCNQ-doped films, indicating that film morphology has a smaller impact on the local mobility of polarons than Coulomb trapping. Although changing the morphology of the film can affect the ratio of free to Coulomb-trapped polarons, there appears to be no easy route to eliminate Coulomb-trapped polarons solely through controlling film morphology. Instead, increasing the polaron-anion distance with a large dopant, like DDB-F_{72}, provides the most direct route for creating delocalized and mobile charge carriers that are not Coulombically trapped.

Supporting Information

Supporting Information is available from the Wiley Online Library or from the author.

Acknowledgements

This work was supported by the National Science Foundation under grants CHE-2305152 and DMR-2513790 and National Science Foundation, Division of Materials Research grant 2513790. A.M.S. thanks NIGMS (R35GM124746) for supporting this work.

Conflict of Interest

The authors declare no conflict of interest.

Data Availability Statement

The data that support the findings of this study are available in the supplementary material of this article.

Keywords

chemical doping, coulomb-trapped polarons, dodecaborane-based dopant, dopant counterion, free polarons, semiconducting polymers

Received: March 24, 2025
Revised: May 19, 2025
Published online:

[1] D. K. Campbell, A. R. Bishop, K. Fesser, *Phys. Rev. B* **1982**, *26*, 6862.
[2] T.-C. Chung, J. H. Kaufman, A. J. Heeger, F. Wudl, *Phys. Rev. B* **1984**, *30*, 702.
[3] J. L. Bredas, G. B. Street, *Acc. Chem. Res.* **1985**, *18*, 309.
[4] M. Nowak, S. D. D. V. Rughooputh, S. Hotta, A. J. Heeger, *Macromolecules* **1987**, *20*, 965.
[5] D. Fichou, G. Horowitz, B. Xu, F. Garnier, *Synth. Met.* **1990**, *39*, 243.
[6] D. Beljonne, J. Cornil, H. Sirringhaus, P. J. Brown, M. Shkunov, R. H. Friend, J.-L. Brédas, *Adv. Funct. Mater.* **2001**, *11*, 229.
[7] O. Bubnova, Z. U. Khan, H. Wang, S. Braun, D. R. Evans, M. Fabretto, P. Hojati-Talemi, D. Dagnelund, J.-B. Arlin, Y. H. Geerts, S. Desbief, D. W. Breiby, J. W. Andreasen, R. Lazzaroni, W. M. Chen, I. Zozoulenko, M. Fahlman, P. J. Murphy, M. Berggren, X. Crispin, *Nature Mater* **2014**, *13*, 190.
[8] S. Kahmann, M. A. Loi, C. J. Brabec, *J. Mater. Chem. C* **2018**, *6*, 6008.
[9] E. C. Wu, B. J. Schwartz, *J. Chem. Theory Comput.* **2023**, *19*, 6761.
[10] D. T. Scholes, P. Y. Yee, J. R. Lindemuth, H. Kang, J. Onorato, R. Ghosh, C. K. Luscombe, F. C. Spano, S. H. Tolbert, B. J. Schwartz, *Adv. Funct. Mater.* **2017**, *27*, 1702654.
[11] R. Ghosh, C. K. Luscombe, M. Hambsch, S. C. B. Mannsfeld, A. Salleo, F. C. Spano, *Chem. Mater.* **2019**, *31*, 7033.
[12] J. Cornil, D. Beljonne, J. L. Brédas, *J. Chem. Phys.* **1995**, *103*, 842.
[13] J. Cornil, J. Brédas, *Adv. Mater.* **1995**, *7*, 295.
[14] C. Wang, D. T. Duong, K. Vandewal, J. Rivnay, A. Salleo, *Phys. Rev. B* **2015**, *91*, 085205.
[15] I. Zozoulenko, A. Singh, S. K. Singh, V. Gueskine, X. Crispin, M. Berggren, *ACS Appl. Polym. Mater* **2019**, *1*, 83.
[16] G. Heimel, *ACS Cent. Sci.* **2016**, *2*, 309.
[17] M. G. Voss, D. T. Scholes, J. R. Challa, B. J. Schwartz, *Faraday Discuss.* **2019**, *216*, 339.
[18] M. G. Voss, J. R. Challa, D. T. Scholes, P. Y. Yee, E. C. Wu, X. Liu, S. J. Park, O. L. Ruiz, S. Subramaniyan, M. Chen, S. A. Jenekhe, X. Wang, S. H. Tolbert, B. J. Schwartz, *Adv. Mater.* **2021**, *33*, 2000228.
[19] A. R. Umar, A. L. Dorris, N. M. Kotadiya, N. C. Giebink, G. S. Collier, C. Grieco, *J. Phys. Chem. C* **2023**, *127*, 9498.
[20] A. R. Umar, A. L. Dorris, C. Grieco, *Adv Funct Materials* **2024**, *34*, 2407181.
[21] A. R. Umar, C. Grieco, *J. Chem. Phys.* **2025**, *162*, 054720.
[22] E. C. Wu, B. J. Schwartz, *J. Chem. Theory Comput.* **2024**, *20*, 10059.
[23] T. J. Aubry, J. C. Axtell, V. M. Basile, K. J. Winchell, J. R. Lindemuth, T. M. Porter, J. Liu, A. N. Alexandrova, C. P. Kubiak, S. H. Tolbert, A. M. Spokoyny, B. J. Schwartz, *Adv. Mater.* **2019**, *31*, 1805647.
[24] T. J. Aubry, K. J. Winchell, C. Z. Salamat, V. M. Basile, J. R. Lindemuth, J. M. Stauber, J. C. Axtell, R. M. Kubena, M. D. Phan, M. J. Bird, A. M. Spokoyny, S. H. Tolbert, B. J. Schwartz, *Adv. Funct. Mater.* **2020**, *30*, 2001800.
[25] E. C. Wu, C. Z. Salamat, O. L. Ruiz, T. Qu, A. Kim, S. H. Tolbert, B. J. Schwartz, *Adv Funct Mater.* **2023**, *33*, 2213652.
[26] D. A. Stanfield, Z. Mehmedović, B. J. Schwartz, *Chem. Mater.* **2021**, *33*, 8489.
[27] R.-Q. Png, M. C. Y. Ang, M.-H. Teo, K.-K. Choo, C. G. Tang, D. Belaineh, L.-L. Chua, P. K. H. Ho, *Nat. Commun.* **2016**, *7*, 11948.
[28] J. C. Axtell, L. M. A. Saleh, E. A. Qian, A. I. Wixtrom, A. M. Spokoyny, *Inorg. Chem.* **2018**, *57*, 2333.
[29] A. D. Ready, Y. A. Nelson, D. F. Torres Pomares, A. M. Spokoyny, *Acc. Chem. Res.* **2024**, *57*, 1310.
[30] Y. Wu, C. Z. Salamat, A. León Ruiz, A. F. Simafranca, N. Akmanşen-Kalayci, E. C. Wu, E. Doud, Z. Mehmedović, J. R. Lindemuth, M. D.

Phan, A. M. Spokoyny, B. J. Schwartz, S. H. Tolbert, *Chem. Mater.* **2024**, *36*, 5552.
[31] T. L. Murrey, T. J. Aubry, O. L. Ruiz, K. A. Thurman, K. H. Eckstein, E. A. Doud, J. M. Stauber, A. M. Spokoyny, B. J. Schwartz, T. Hertel, J. L. Blackburn, A. J. Ferguson, *Cell Reports Physical Science* **2023**, *4*, 101407.
[32] E. M. Thomas, K. A. Peterson, A. H. Balzer, D. Rawlings, N. Stingelin, R. A. Segalman, M. L. Chabinyc, *Adv. Electron. Mater.* **2020**, *6*, 2000595.
[33] C. Chen, I. E. Jacobs, K. Kang, Y. Lin, C. Jellett, B. Kang, S. B. Lee, Y. Huang, M. BaloochQarai, R. Ghosh, M. Statz, W. Wood, X. Ren, D. Tjhe, Y. Sun, X. She, Y. Hu, L. Jiang, F. C. Spano, I. McCulloch, H. Sirringhaus, *Adv. Energy Mater.* **2023**, *13*, 2202797.
[34] K. N. Baustert, J. H. Bombile, M. T. Rahman, A. O. Yusuf, R. Li, A. J. Huckaba, C. Risko, K. R. Graham, *Adv. Mater.* **2024**, *36*, 2313863.
[35] O. G. Reid, R. D. Pensack, Y. Song, G. D. Scholes, G. Rumbles, *Chem. Mater.* **2014**, *26*, 561.
[36] D. T. Scholes, S. A. Hawks, P. Y. Yee, H. Wu, J. R. Lindemuth, S. H. Tolbert, B. J. Schwartz, *J. Phys. Chem. Lett.* **2015**, *6*, 4786.
[37] I. E. Jacobs, E. W. Aasen, J. L. Oliveira, T. N. Fonseca, J. D. Roehling, J. Li, G. Zhang, M. P. Augustine, M. Mascal, A. J. Moulé, *J. Mater. Chem. C* **2016**, *4*, 3454.
[38] J. C. Aguirre, S. A. Hawks, A. S. Ferreira, P. Yee, S. Subramaniyan, S. A. Jenekhe, S. H. Tolbert, B. J. Schwartz, *Adv. Energy Mater.* **2015**, *5*, 1402020.
[39] A. R. Chew, R. Ghosh, Z. Shang, F. C. Spano, A. Salleo, *J. Phys. Chem. Lett.* **2017**, *8*, 4974.
[40] C. Zhang, Y. Hu, A. Tang, Z. Deng, F. Teng, *J of Applied Polymer Sci* **2015**, *132*, 41757.
[41] M. T. Fontana, H. Kang, P. Y. Yee, S. A. Hawks, L. T. Schelhas, S. Subramaniyan, Y.-J. Hwang, S. A. Jenekhe, S. H. Tolbert, B. J. Schwartz, *Materials and Energy* **2018**, *122*, 16574.
[42] M. T. Fontana, D. A. Stanfield, D. T. Scholes, K. J. Winchell, S. H. Tolbert, B. J. Schwartz, *J. Phys. Chem. C* **2019**, *123*, 22711.
[43] X. Jiao, M. Statz, L. Lai, S. Schott, C. Jellett, I. McCulloch, H. Sirringhaus, C. R. McNeill, *J. Phys. Chem. B* **2020**, *124*, 10529.
[44] P. Das, C. Z. Salamat, B. Zayat, R. Elizalde-Segovia, Y. Wang, X. Gu, S. R. Narayan, S. H. Tolbert, B. C. Thompson, *Chem. Mater.* **2024**, *36*, 1413.
[45] S. A. Gregory, R. Hanus, A. Atassi, J. M. Rinehart, J. P. Wooding, A. K. Menon, M. D. Losego, G. J. Snyder, S. K. Yee, *Nat. Mater.* **2021**, *20*, 1414.
[46] S. D. Kang, G. J. Snyder, *Nature Mater* **2017**, *16*, 252.
[47] P. Roy, G. T. Anandan, N. Nayak, A. Kumar, J. Dasgupta, *J. Phys. Chem. B* **2023**, *127*, 567.